

Transient response of vibration systems with viscous-hysteretic mixed damping using Hilbert transform and effective eigenvalues

S.H. Bae¹, W.B. Jeong^{*2}, J.R. Cho³ and J.H. Lee¹

¹Nuclear EQ and Safety Center, Korea Institute of Machinery and Materials, Busan 467-44, Korea

²School of Mechanical Engineering, Pusan National University, Busan 609-735, Korea

³Department of Naval Architecture and Ocean Engineering, Hongik University, Sejong 339-701, Korea

(Received January 2, 2017, Revised June 22, 2017, Accepted June 25, 2017)

Abstract. This paper presents the time response of a mixed vibration system with the viscous damping and the hysteretic damping. There are two ways to derive the time response of such a vibration system. One is an analytical method, using the contour integral of complex functions to compute the inverse Fourier transforms. The other is an approximate method in which the analytic functions derived by Hilbert transform are expressed in the state space representation, and only the effective eigenvalues are used to efficiently compute the transient response. The unit impulse responses of the two methods are compared and the change in the damping properties which depend on the viscous and hysteretic damping values is investigated. The results showed that the damping properties of a mixed damping vibration system do not present themselves as a linear combination of damping properties.

Keywords: viscous-hysteretic mixed damping (VHMD); transient response; unit impulse response; effective eigenvalues; Hilbert transform; state space

1. Introduction

The most widely used forms of linear damping in the modeling of damping systems are viscous damping and hysteretic damping. The responses in viscous damping have been widely studied while the constant complex stiffness has been typically used for the responses of hysteretic damping. When such hysteretic properties are kept constant regardless of the frequency, the system is taken as a constant hysteretic damping system and a constant complex number is set as the stiffness.

An example of a constant hysteretic damping model is a layered structure made with viscoelastic materials, in which a complex shear factor is used to express the energy dissipation through the shear strains of viscoelastic layers (Genta and Amati 2010, Zhu *et al.* 2014, Akbas 2016). This concept can be applied to the properties of a variety of materials. For the structures with complex stiffness, the frequency analysis can be done by numerical methods. When constructing the finite element modeling to deduce the response of a 3-layered beam with complex stiffness, the system's frequency response can be computed by approximating the strain energy of beam with the shape functions of displacement (Won *et al.* 2013, Amichi and Atalla 2009). Additionally, the frequency response of the beams coated with damping materials can be computed by applying the Timoshenko beam model to derive the beam's equivalent complex stiffness (Won *et al.* 2012).

There are many models for hysteretic damping and each model uses different definition, but it is important to adopt the most appropriate hysteretic damping model for a given system. Soroka (2012) defined the system eigenvalue as the complex number, which is shown as the complex stiffness, and expressed the complex stiffness as a viscous damping term. In this case, most of analyses are conducted in the frequency domain.

On the other hand, when analyzing the structural impulse problem, it is important to find out the system's maximum displacement in the time domain. Therefore, the transient response has to be obtained. As described earlier, the complex stiffness is defined in the frequency domain, and thus the time response cannot be obtained directly in the frequency domain. In such case, the most widely used method is to apply the inverse Fourier transform to the transfer function defined in the frequency domain to obtain the time response (Nashif *et al.* 1985). For the unit impulse response in a single degree of freedom complex coefficient (hysteretic) system, Gaul *et al.* (1985) proposed a method in which the complex plane contour integral is used to conduct the inverse Fourier transform. There also exists a numerical method in which the governing equations of the complex stiffness problem are expressed as integral equations in the time domain and the time responses are obtained from them (Chen and You 1999). In a single degree of freedom complex damping system, Laplace transform can also be used (Bonisoli and Mottershead 2004, Mohammadi and Sedaghati 2012). In such a case, the system's response has non-casual effect (Crandall 1970)

Despite of these problems, the numerical IFT method can be used to obtain the relatively accurate responses when the time domain is designated and the excitation forces with

*Corresponding author, Professor
E-mail: wbyeong@pusan.ac.kr

appropriate zero extension are applied, so that the periodic nature of the discrete Fourier transforms does not appear (Bae *et al.* 2014). Barkanov *et al.* (2000) used the numerical IFT method to obtain time responses of the laminated beam with elastic and damping layers which is subjected to arbitrary excitation force. A similar numerical method that can be applied is the time reversal method (Inaudi and Makis 1996, Li *et al.* 2012, Padois *et al.* 2012, Wang *et al.* 2015). However, the abovementioned two methods have a common difficulty in identifying the appropriate initial conditions for solving the time responses. If the time responses are obtained using the analytical method, then the responses to the initial conditions can be obtained. But, this method becomes less convenient to use because the time responses are expressed in the integral form.

To resolve the problems associated with the transient response in state space and the initial conditions, we in the previous study (Bae *et al.* 2014) separated the governing equations of the complex stiffness system, which is defined by analytic signals through Hilbert transform, into two complex governing equations. In this approach, we applied the hypothesis that the free vibration of the system converges with the lapse of time due to damping. Henwood (2002) did also propose the modeling method using the system's equivalent viscous damping to deal with such hysteretic models in the time domain. The purpose of current study is to extend our previous study to examine the characteristics and to obtain the time response of a mixed system with complex stiffness and viscous damping, in the state space and the frequency domain. Because the response convergence conditions that were used in the previous study cannot be applied to obtain the free vibration in state space, the current study focuses on the relationship between the eigenvalues of the state space and the poles of transfer functions.

We first obtain the unit impulse responses in the frequency domain through the contour integral. And then, among the four eigenvalues which were obtained in state space, we determine the effective eigenvalues that affect the actual impulse response to obtain the system's free vibration response. After that, the damping properties and the damped natural frequencies of the responses are investigated with respect to the complex stiffness and viscous damping, and their relationship is examined. Finally, the obtained single degree of freedom free vibration responses are used to obtain the transient time response of a mixed vibration system with viscous and hysteretic damping.

2. Governing equation of viscous-hysteretic damping system

A system with both viscous damping and complex stiffness includes both hysteretic damping properties and viscous damping in its material properties. If a structure with structural damping properties is installed with a viscous damping mount, it can be thought as an example of a viscous-complex stiffness system.

Fig. 1 shows a schematic diagram of a mixed system with viscous damping and complex stiffness. According to

Inaudi and Makis (1996), the equations of motion is given by

$$m\ddot{x}(t) + c\dot{x}(t) + kx(t) - \frac{k\eta}{\pi} \int_{-\infty}^{\infty} \frac{x(\tau)}{t-\tau} d\tau = f(t) \quad (1)$$

Here, we introduce the Hilbert transform of $x(t)$, which is defined by

$$y(t) = \frac{1}{\pi} \int_{-\infty}^{\infty} \frac{-x(\tau)}{t-\tau} d\tau \quad (2)$$

Then, the Fourier transform of Eq. (2) becomes (Bae *et al.* 2014)

$$FT[y(t)] = Y(\omega) = i \operatorname{sgn}(\omega) X(\omega) \quad (3)$$

with $X(\omega)$ and $Y(\omega)$ being the Fourier transforms of $x(t)$ and $y(t)$, respectively. Here, the value of $i \operatorname{sgn}(\omega)$ is as follows: i ($\omega > 0$), 0 ($\omega = 0$) and $-i$ ($\omega < 0$). By taking Fourier transform to Eq. (1) and using the relation (3), one can get

$$-\omega^2 mX(\omega) + i\omega cX(\omega) + kX(\omega) + ik\eta \operatorname{sgn}(\omega)X(\omega) = F(\omega) \quad (4)$$

Multiplying Eq. (4) by $i \operatorname{sgn}(\omega)$ and using the relation (3), it is not hard to follow that Eq. (4) ends up with (Johansson 1999)

$$-\omega^2 mY(\omega) + i\omega cY(\omega) + kY(\omega) - k\eta X(\omega) = \hat{F}(\omega) \quad (5)$$

Where, $\hat{F}(\omega)$ is the Fourier Transform of the Hilbert transform of $f(t)$.

We next define the analytic signal $z_a(t)$ as

$$z_a = x(t) - iy(t) \quad (6)$$

Let us take the inverse Fourier transform to Eqs. (4) and (5) and multiply Eq. (5) by the negative imaginary number $-i$. After that, combining the resulting two equations ends up with the following time-domain governing equation that is expressed in terms of the analytic signal $z_a(t)$ in a viscous complex-stiffness system

$$\ddot{z}_a(t) + 2\xi\omega_n \dot{z}_a(t) + \omega_n^2(1 + i\eta)z_a(t) = f_a(t)/m \quad (7)$$

Here, $\xi = c/(2\sqrt{mk})$ is the viscous damping ratio, η the loss factor, and $\omega_n = \sqrt{k/m}$ the undamped natural frequency.

Separating the real and imaginary parts of the governing equation of the viscous damping-complex stiffness system, Eq. (7) is divided into two differential equations given by

$$\begin{aligned} \ddot{x}(t) + 2\omega_n\xi\dot{x}(t) + \omega_n^2x(t) - \eta\omega_n^2y(t) &= f(t)/m \\ \ddot{y}(t) + 2\omega_n\xi\dot{y}(t) + \eta\omega_n^2x(t) + \omega_n^2y(t) &= \hat{f}(t)/m \end{aligned} \quad (8)$$

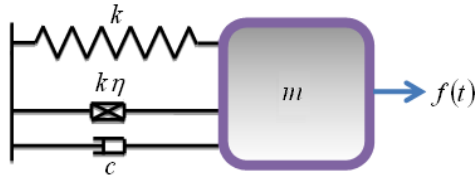


Fig. 1 Viscous-hysteretic damped system

3. Analytical method using inverse Fourier transform

3.1 Complex integration method

When the system of 2nd order differential equations given in Eq. (8) is put into the eigen decomposition in state space, then four eigenvalues will come out. The unit impulse response of the viscous damping-complex stiffness system can be obtained by taking the inverse Fourier transform of the transfer function $X(\omega)/F(\omega)$ given in Eq. (4), which is given by

$$mg(t) = \frac{1}{2\pi} \int_{-\infty}^{\infty} \frac{e^{i\omega t}}{[\omega_n^2(1+i\eta \operatorname{sgn}(\omega)) + i2\xi\omega_n\omega - \omega^2]} d\omega \quad (9)$$

The poles of transfer function of such a system can be obtained by substituting the denominator in Eq. (9) into the quadratic formula

$$\text{Pole} = i\omega_n\xi \pm \omega_n\sqrt{1-\xi^2 + i\eta \operatorname{sgn}(\omega)} \quad (10)$$

One can see that poles are expressed as complex numbers in square roots. When the poles are marked on a complex plane, as shown in Fig. 2, they can be rewritten as

$$\text{Pole} = \sigma i \pm (b - ia \operatorname{sgn}(\omega)) \quad (0 < \xi < 1) \quad (11)$$

Where, a and b are

$$a = \omega_n \sqrt{\sqrt{(1-\xi^2)^2 + \eta^2} - (1-\xi^2)} / \sqrt{2} \quad (12)$$

$$b = \omega_n \sqrt{\sqrt{(1-\xi^2)^2 + \eta^2} + (1-\xi^2)} / \sqrt{2}$$

The poles of transfer function which are expressed in Eq. (10) indicate a vertical shift of $\pm(b + ia \operatorname{sgn}(\omega))$ by σi along the imaginary-axis on the complex plane. Therefore, if σi is larger than ia , then the poles lie on the upper half-plane, appearing as if the effective extreme values are four. In order to identify the effective poles which are used for the integration, we need to define the path of contour integral.

When ξ is $0 < \xi < 1$, the contour including the integration defined in Eq. (9) is defined as two closed quarter circles and is identical to the contour for obtaining the unit impulse response of a complex stiffness system (Bae *et al.* 2014). Two closed contour integrals are represented in Fig. 2, where C_k refers to the k -th

integral contour

When ω is a positive number, the poles of the system appear on the 1st quadrant and 3rd quadrant or on the 2nd quadrant (when $\sigma > a$) of the complex plane. But, since ω is positive, the effective pole used for the integration is located on the 1st quadrant. Similarly, when ω is negative, the poles lie on the 2nd quadrant and 4th quadrant or on the 1st quadrant (when $\sigma > a$). However, in this case, the contour integral only includes the effective pole located on the 2nd quadrant. Therefore, only the poles located on the 1st ($\omega > 0$) and 2nd ($\omega < 0$) quadrants are used for integration, regardless of σ or a . If the contour integration is conducted along $\omega < 0$ and $\omega > 0$, the sum becomes 0

$$\int \frac{mX(\omega)}{F(\omega)} e^{i\omega t} dz = mg(t) + \sum_{k=2}^{10} \int_{C_k} \frac{mX(\omega)}{F(\omega)} e^{i\omega t} dz = 0 \quad (13)$$

according to the Cauchy's integral theorem. In the above Eq. (13), the unit impulse response $mg(t)$ is the sum of C_1 in each contour. The C_5 converges to 0 when $r \rightarrow \infty$ on the upper half-plane according to Jordan's lemma (Arfken and Weber 2005). The sums of $C_2 + C_4$ and $C_7 + C_9$, also become 0 as they are in the opposite direction and take the same contour. As for the problem in which C_1 is not defined at $\omega = 0$, unlike Eq. (9), C_1 can be ignored because the integral value of the transfer function comes close to 0 when the two domains become very close to 0, when $\omega = 0$, and when the transfer function has a finite value. Therefore, only the contour integrals of C_3, C_6, C_8 and C_{10} contribute to the integration and thus the unit impulse response becomes

$$mg(t) = -(I_3 + I_6 + I_8 + I_{10}) \quad (14)$$

according to the residue theorem. Here, I_k indicates the contour integral along the k -th contour.

The contour integral $I_3 + I_8$ can be obtained using the residue of the poles $\pm b + i(a + \sigma)$ on the 1st ($\omega > 0$) and 2nd ($\omega < 0$) quadrants, which is given by

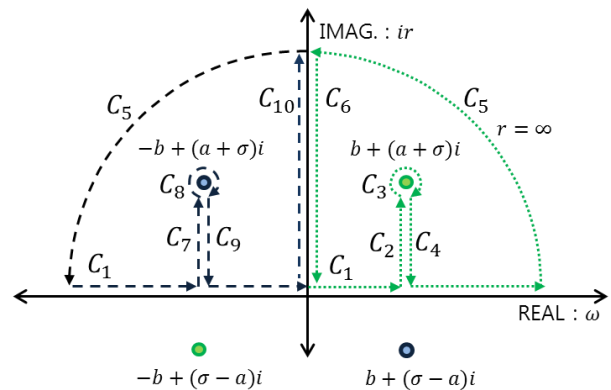


Fig. 2 Unit impulse response integral contours for viscous-hysteretic damped system

$$I_3 + I_8 = -\frac{e^{-(a+\sigma)t}(b \sin(bt) - a \cos(bt))}{(a^2 + b^2)} \quad (15)$$

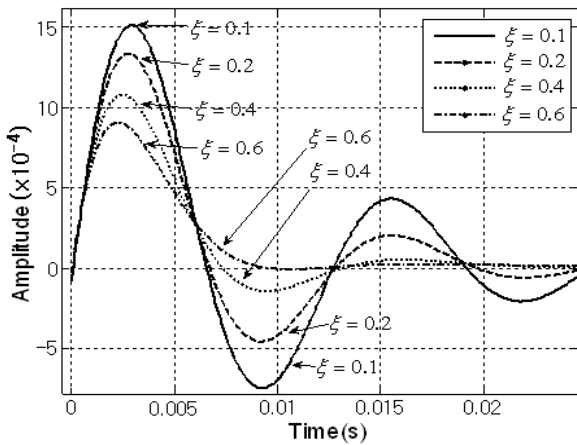
Meanwhile, the complex integrations of the remaining contours C_6 and C_{10} become

$$I_6 = \frac{1}{2\pi} \int_{-\infty}^0 \frac{ie^{-r}}{\omega_n^2 + r^2 - 2\omega_n \xi r - i\omega_n^2 \eta} dr \quad (16)$$

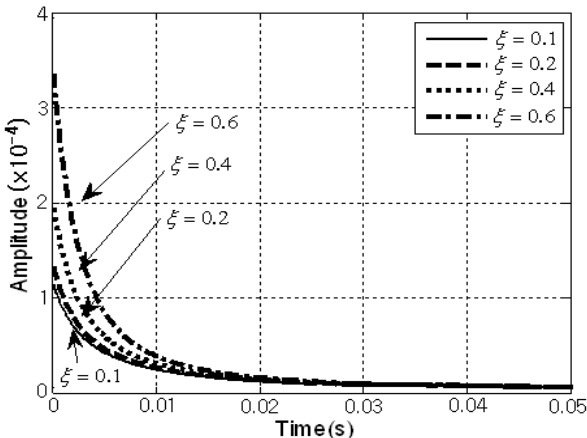
$$I_{10} = \frac{1}{2\pi} \int_0^{\infty} \frac{ie^{-r}}{\omega_n^2 + r^2 - 2\omega_n \xi r + i\omega_n^2 \eta} dr$$

by letting ω in Eq. (9) be ir . Thus, the contour integral $I_6 + I_{10}$ becomes the residual which is defined in the form of Laplace transform of $f(r)$

$$I_6 + I_{10} = -\frac{\omega_n^2 \eta}{\pi} \int_0^{\infty} \frac{e^{-r}}{(\omega_n^2 + r^2 - 2\omega_n \xi r)^2 + (\omega_n^2 \eta)^2} dr \quad (17)$$

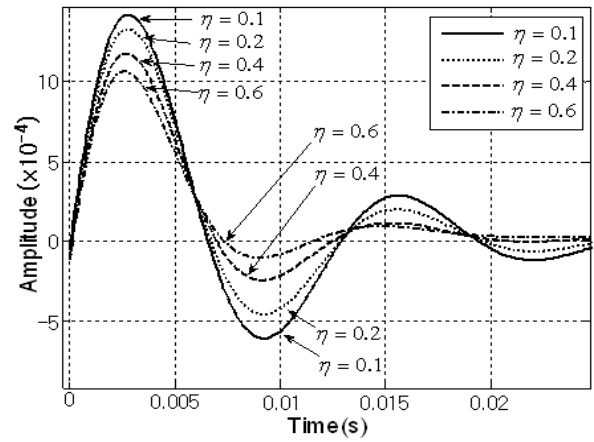


(a) unit impulse response $mg(t)$

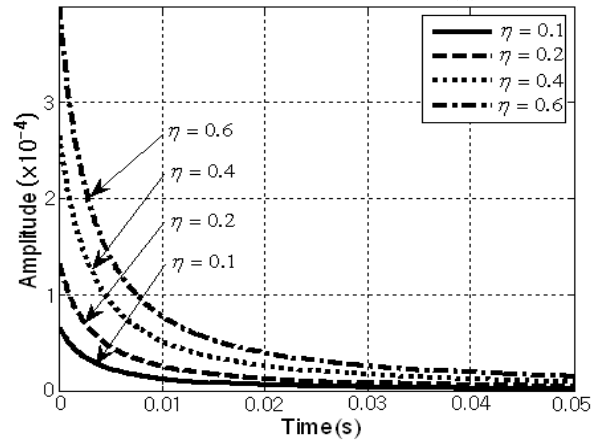


(b) residual term $-(I_6 + I_{10})$

Fig. 3 The responses of viscous-hysteretic damped system obtained by analytic IFT for different ξ ($\eta = 0.2$)



(a) unit impulse response $mg(t)$



(b) residual term $-(I_6 + I_{10})$

Fig. 4 The responses of viscous-hysteretic damped system obtained by analytic IFT for different η ($\xi = 0.2$)

In Eq. (17), the power ratio of the numerator and denominator terms in the integral is to the fourth power, so it is guaranteed to have a relatively higher level of convergence. But, the value of $I_6 + I_{10}$ is smaller than $I_3 + I_8$. The above analytical solutions (15) and (16) in the form of Laplace transform can be calculated by applying the numerical integration to their discretized equations for each integration segments.

3.2 Example of unit impulse response analysis

The unit impulse response $mg(t)$ of a viscous damping-complex stiffness system can be obtained by summing Eqs. (15) and (17) and by adding a negative symbol. Fig. 3 represents the unit impulse response $mg(t)$ and the residual $-(I_6 + I_{10})$ with respect to the viscous damping ratio ξ , in which the loss factor η is set by 0.2.

It can be shown that the larger the damping ratio, the smaller the amplitude of unit impulse response and the

shorter the time taken for the first waveform to reach the peak value. The residual also increases gradually as the viscous damping ratio increases. Fig. 4 shows the unit impulse response $mg(t)$ and the residual $-(I_6+I_{10})$ with respect to the loss factor η when the viscous damping ratio ξ is fixed by 0.2. As the loss factor increases, the waveform shrinks in size, and the width of decrease is sensitive to the change of loss factor. The peak value of the residual increases in proportional to the loss factor, and the width of increase is sensitive to the change of loss factor. From the comparison of Figs. 3 and 4, it is found that the viscous damping ratio has larger effect on the unit impulse response, while the loss factor gives more effect on the residual.

4. Approximation using effective eigenvalues

4.1. State space analysis

This section describes the behavior of the real and imaginary parts of the time-invariant equation of motion in Eq. (7) and demonstrates the use of state space for more simplified handling of the initial value problem that could not be considered in the numerical inverse transform. Eq. (8) which was derived from the Hilbert transform relationship between $x(t)$ and $y(t)$ can be expressed in the matrix form using the state space techniques as following

$$\dot{\mathbf{p}} = \mathbf{A}\mathbf{p} + \mathbf{w} \tag{18}$$

$$\mathbf{A} = \begin{bmatrix} 0 & 1 & 0 & 0 \\ -\omega_n^2 & -2\xi\omega_n & \eta\omega_n^2 & 0 \\ 0 & 0 & 0 & 1 \\ -\eta\omega_n^2 & 0 & -\omega_n^2 & -2\xi\omega_n \end{bmatrix} \tag{19}$$

$$\mathbf{p} = \begin{Bmatrix} x \\ \dot{x} \\ y \\ \dot{y} \end{Bmatrix}, \quad \mathbf{w} = \begin{Bmatrix} 0 \\ f(t)/m \\ 0 \\ \hat{f}(t)/m \end{Bmatrix}$$

with \mathbf{w} being the external force vector. The matrix equation system (18) can be converted into the independent coordinates in state space through the eigen decomposition. When the mode decomposition is applied to Eq. (18), the system's eigenvalue λ and eigenvector \mathbf{V} can be obtained. There are a total of four system eigenvalues in state space and a 4×4 mode matrix.

When an ordinary matrix is mode decomposed, a conjugate relationship is satisfied between the eigenvalue and the eigenvector. As well, the mode vector and the eigenvalue form a complex conjugate relationship. Substituting the eigenvector \mathbf{V} obtained from the eigenvalue problem into Eq. (18) and rewriting in the mode coordinates \mathbf{q} ($\mathbf{p} = \mathbf{V}\mathbf{q}$), together with $\mathbf{A}\mathbf{V} = \lambda\mathbf{V}$, one can get four orthogonalized ordinary differential equations

given by

$$\dot{\mathbf{p}} = \mathbf{A}\mathbf{p} + \mathbf{w} \tag{20}$$

with

$$\lambda = \begin{bmatrix} \lambda_1 & 0 & 0 & 0 \\ 0 & \bar{\lambda}_1 & 0 & 0 \\ 0 & 0 & \lambda_2 & 0 \\ 0 & 0 & 0 & \bar{\lambda}_2 \end{bmatrix}$$

$$\mathbf{V} = \begin{bmatrix} -i/\lambda_1 & i/\bar{\lambda}_1 & i/\lambda_2 & -i/\bar{\lambda}_2 \\ -i & i & i & -i \\ 1/\lambda_1 & 1/\bar{\lambda}_1 & 1/\lambda_2 & 1/\bar{\lambda}_2 \\ 1 & 1 & 1 & 1 \end{bmatrix} \tag{21}$$

$$\phi = \mathbf{V}^{-1}\mathbf{w}$$

Where, $\lambda_1 = -\sigma + a + ib$, $\lambda_2 = -\sigma - a + ib$ and $\sigma = \xi\omega_n$ when $0 < \xi < 1$, while $\lambda_1 = ib$ and $\lambda_2 = -2\sigma + ib$ when $\eta = 2\xi$. Here, ϕ is the external force vector in the mode coordinates. The real and imaginary parts of the computed eigenvalues λ are expressed in terms of the loss factor η , viscous damping ratio ξ , and eigen frequency ω_n . The four eigenvalues obtained from Eq. (20) directly reflect the extreme values of the system which is defined in the previous transfer function in Eq. (9). Here, in the similar manner for obtaining the unit impulse responses by the inverse Fourier transform in Section 3.1 using only two of four extreme values, we carry out the approximation for integration in the state space using only λ_2 and $\bar{\lambda}_2$ which influence the actual response transfer functions, in order to obtain the unit impulse responses.

The free vibration response solution $x(t)$ in the 1st order ordinary differential equation (where $\phi = 0$) is expressed in the following form of exponential function

$$q_1(t) = c_1 e^{\lambda_1 t} \tag{22}$$

Using Eq. (20) (i.e., the response in the mode coordinates) and Eq. (22) (i.e., the free vibration response in first-order differential equation), the responses in the generalized coordinates are as follows

$$\mathbf{p}(t) = C_1 \mathbf{V}_1 e^{\lambda_1 t} + \bar{C}_1 \bar{\mathbf{V}}_1 e^{\bar{\lambda}_1 t} + C_3 \mathbf{V}_3 e^{\lambda_2 t} + \bar{C}_3 \bar{\mathbf{V}}_3 e^{\bar{\lambda}_2 t} \tag{23}$$

Here, \mathbf{V}_n refers to the n^{th} column vector in the mode matrix \mathbf{V} and $C_1 = c_1 + ic_2$, $C_3 = c_3 + ic_4$ are complex constants. From Eq. (23), if we select the eigenvalue to be used, then the resulting system response becomes (Bae *et al.* 2014)

$$\mathbf{p}(t) = C_3 \mathbf{V}_3 e^{\lambda_2 t} + \bar{C}_3 \bar{\mathbf{V}}_3 e^{\bar{\lambda}_2 t} \tag{24}$$

Using the Euler theorem to convert Eq. (24) into the form of trigonometric function and rearranging the equation

leads to

$$\mathbf{p}(t) = e^{-(\sigma+a)t} [\text{Re}[\mathbf{V}_3](2c_3 \cos(bt) - 2c_4 \sin(bt)) - \text{Im}[\mathbf{V}_3](2c_4 \cos(bt) + 2c_3 \sin(bt))] \quad (25)$$

Eq. (25) becomes $\mathbf{p}(0) = \{x_0, \dot{x}_0, y_0, \dot{y}_0\}^T = 2c_3 \text{Re}[\mathbf{V}_3] - 2c_4 \text{Im}[\mathbf{V}_3]$ at $t=0$, from which four unknowns (i.e., c_3, c_4, y_0 and \dot{y}_0) can be determined in terms of the given real initial conditions x_0, \dot{x}_0 and the three constants σ, a and b in $\lambda 2$ (Bae *et al.* 2014). By substituting c_3 and c_4 into Eq. (25) and arranging with respect to the real and imaginary initial conditions, one can get

$$\mathbf{p}(t) = \begin{Bmatrix} x \\ \dot{x} \\ y \\ \dot{y} \end{Bmatrix} = e^{-(\sigma+a)t} \begin{bmatrix} \cos(bt) & 0 & -\sin(bt) & 0 \\ 0 & \cos(bt) & 0 & -\sin(bt) \\ \sin(bt) & 0 & \cos(bt) & 0 \\ 0 & \sin(bt) & 0 & \cos(bt) \end{bmatrix} \begin{Bmatrix} x_0 \\ \dot{x}_0 \\ y_0 \\ \dot{y}_0 \end{Bmatrix} \quad (26)$$

with the determined imaginary initial conditions $y_0 = -(\dot{x}_0 + x_0(a + \sigma)) / b$ and $\dot{y}_0 = (x_0((a + \sigma)^2 + b^2) + \dot{x}_0(a + \sigma)) / b$. The real and imaginary parts in Eq. (26) form a Hilbert transform relationship and a Kramers-Kronig relationship (Feldman, 2011).

effective eigenvalues ($\omega_n = 500 \text{ rad / s}$)

The above Eq. (26) is in the form of a viscous damping free vibration response and constitutes an approximation of the system in the form of viscous damping using the effective eigenvalues. When using the free vibration response to obtain the unit impulse response $g(t)$, the initial conditions are set by $x(0)=0, \dot{x}(0)=1$ and the results are given by

$$g(t) = \frac{1}{b} e^{-(\sigma+a)t} \sin(bt) \quad (27)$$

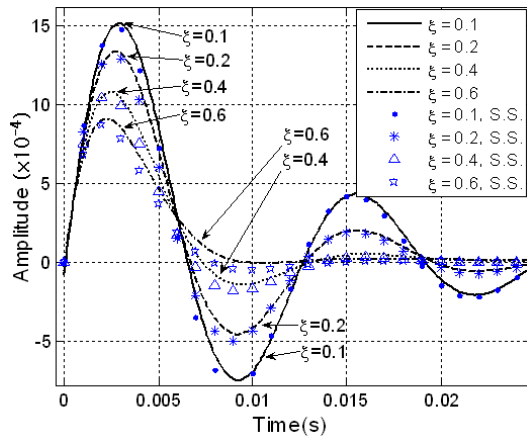
The unit impulse response $g(t)$ contains two exponential terms $e^{-\sigma t}$ and e^{-at} . The former is the viscous damping, while the latter is a combination of hysteretic damping and viscous damping. The unit impulse response vibrates at the damped eigen frequency b which represents the imaginary number part of the state space eigenvalue. Meanwhile, the forced vibration response can be obtained by the convolution integral of the unit impulse response and external force. When the free vibration response is added, the general time response is expressed by

$$x(t) = \int_0^t f(\tau) g(t-\tau) d\tau + x_0 \cos(\omega t) + y_0 \sin(\omega t) \quad (28)$$

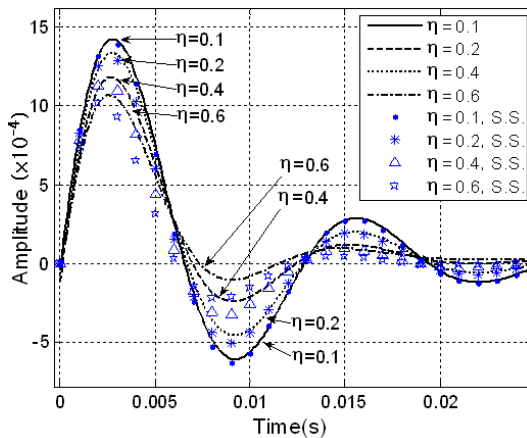
When Eq. (28) is numerically integrated through discretization, the time responses to ordinary excitation forces can be obtained. The reader may refer to our previous paper (Bae *et al.* 2016) for the details of the numerical integration method.

4.2 Example of unit impulse response analysis

The unit impulse responses obtained by IFT using Eq. (14) in the frequency domain and those approximated in state space using Eq. (27) are compared in Fig. 5. The natural frequency of the responses is 500 rad/s . In Fig. 5(a), η is fixed by 0.2 while ξ is varying to compare the unit impulse responses. In this case, it is observed that both cases show similar unit impulse responses when ξ is small. But, it is also shown that the difference between two methods increases in proportion to ξ . Meanwhile, Fig. 5(b) compares the unit impulse responses when ξ is fixed by 0.2 while η is varying. Similar to Fig. 5(a), the discrepancy between two methods increases in proportion to η . But, the level of discrepancy between two methods is shown to be larger, when compared with Fig. 5(a). This is because when the unit impulse response of a viscous damping system is approximated in state space, the system becomes closer to a hysteretic damping system than it does to a viscous damping system, as the damping coefficient increases. Therefore, the approximation of system using state space becomes more accurate when the viscous damping is larger than the structural damping or when the system is a low damping system.

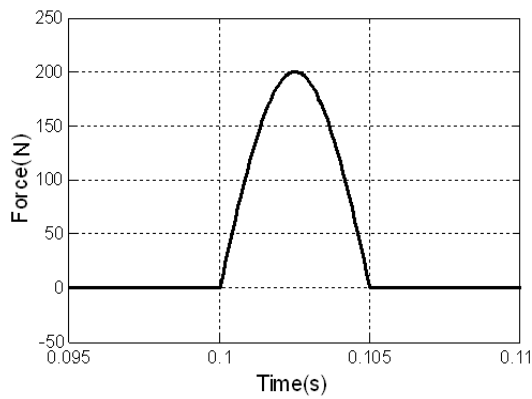


(a) for constant $\eta = 0.2$

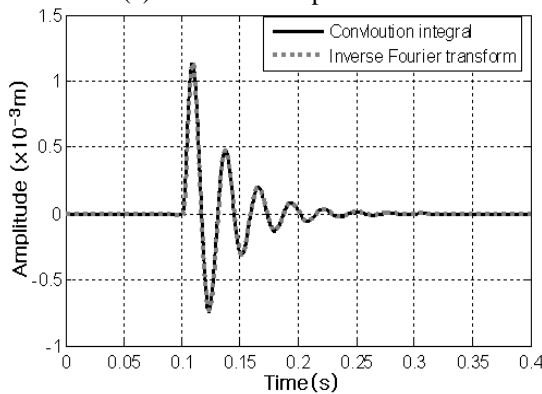


(b) for constant $\xi = 0.2$

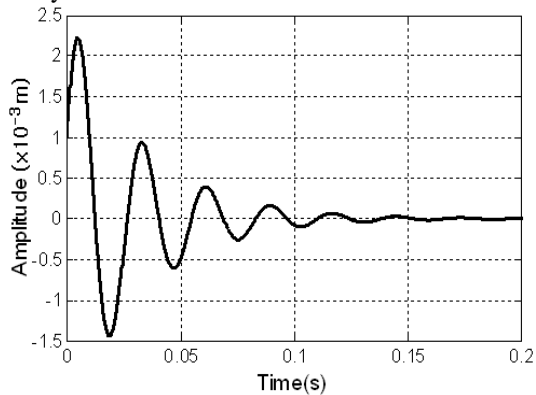
Fig. 5 Comparison of the unit impulse responses between IFT and the state space (S.S.) analysis using



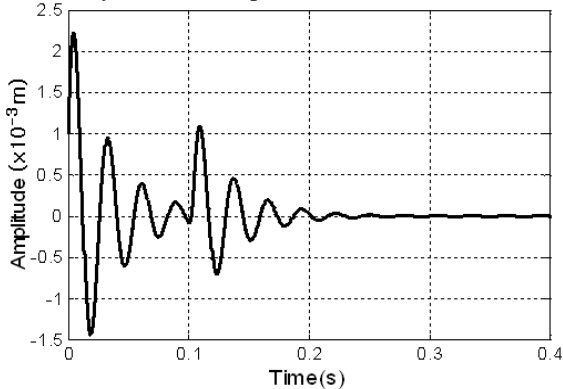
(a) A half-sine impulse force



(b) the system forced vibration without initial conditions



(c) the system free response with initial conditions



(d) the system response when both the impulse force and the initial conditions are applied.

Fig. 6 The state space (S.S.) force vibration analysis using effective eigenvalues

4.3 Example of forced vibration response analysis

The forced vibration response, the initial condition response and the response by considering both the forced vibration and the initial conditions were obtained for a single degree of freedom complex stiffness-viscous damping system. The system mass is $m = 2\text{kg}$, the spring constant is $k = 1 \times 10^5 \text{ N/m}$, the loss factor is $\eta = 0.05$, and the viscous damping coefficient is $c = 100 \text{ Ns/m}$. Fig. 6(a) shows a half-sine impulse force, while Fig. 6(b) compares the forced vibration responses to the impulse force between the convolution integral method (28) and IFT when the initial conditions are not specified. Fig. 6(c) shows the free vibration response of system when the initial conditions of $x(0) = 10^{-4} \text{ m}$ and $\dot{x}(0) = 0.5 \text{ m/s}$ are specified. The final Fig. 5(d) represents the response when both the impulse force and initial conditions are applied. In order to verify the present convolution integral method (28), the comparison was made as shown in Fig. 6(b), where the plot labeled by IFT was obtained by superposing the unit impulse responses obtained through the inverse Fourier transform (Bae *et al.* 2014). It is clearly observed that the present method is in an excellent agreement with IFT. Furthermore, from Figs. 6(c) and 6(d), it is found that this method can accurately implement the initial conditions and solve the forced vibration response by specifying the initial conditions. Thus, it has been justified that this method can provide the accurate transient response of viscous-hysteretic mixed damping system.

Next, the forced vibration response of a cantilever Euler beam shown in Fig. 7 with complex stiffness-viscous damping is considered. The length L is 0.25 m and the dimensions of beam cross-section are $b = 0.04 \text{ m}$ and $h = 0.02 \text{ m}$, while the density ρ and the Young's modulus E are $2,705 \text{ kg/m}^3$ and $69.0 \times 10^9 \text{ N/m}^2$, respectively. The neutral axis of beam is uniformly divided into five elements and five active nodes. The total degrees of freedom (DOFs) are 10 because each node has two DOFs (i.e., $x = (w, dw/dx)$). Hermite basis functions are used for the spatial approximation of the vertical displacement $w(x, t)$ of beam.

A double half-sine impulse force $f(t)$ shown in Fig. 8(a) is applied to node 3, and the real part of initial conditions are set by $w(0) = \dot{w}(0) = 0$.

With twenty effective complex eigenvalues and eigenvectors, the ten nodal transient responses of $(w, dw/dx)$ were approximated using the state space analysis method introduced in Section 4.1. Fig 8(b) compares the transient responses of the vertical displacement w at node 2 between the present method and the inverse Fourier transform.

An excellent agreement is clearly observed, which justifies that the proposed method does also provides the accurate transient response of MDOF viscous-hysteretic mixed damping system.

represents the system's total damping. In order to justify

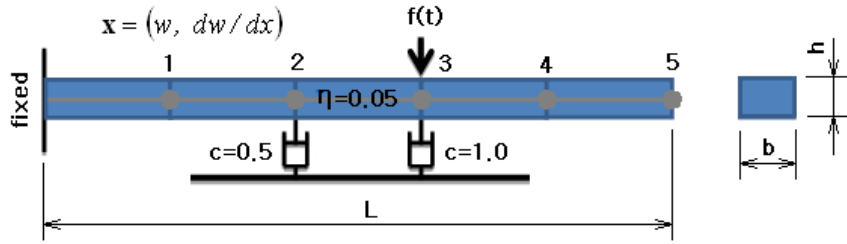


Fig. 7 A 10-DOF Euler beam model with complex stiffness-viscous damping

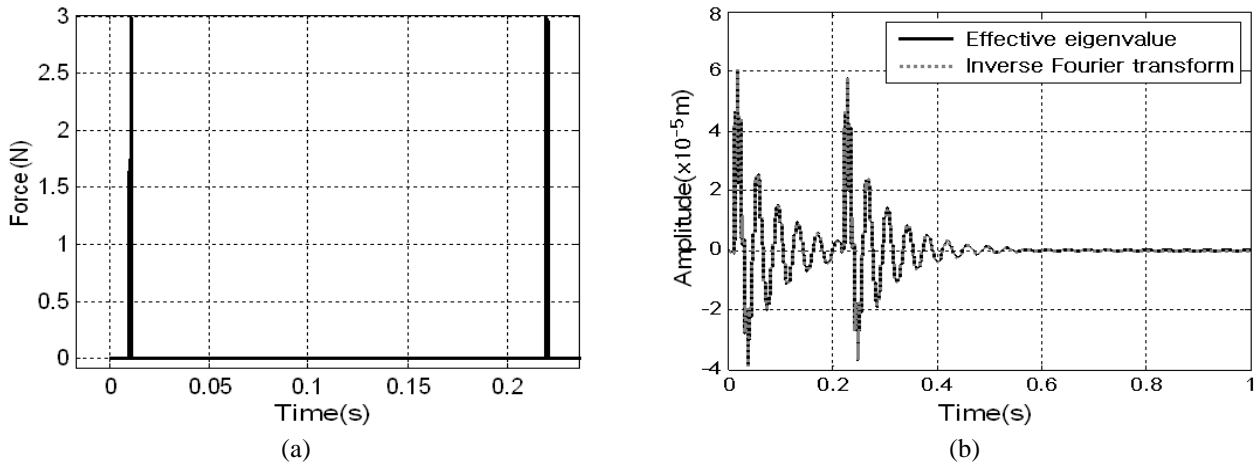


Fig. 8 (a) A double half-sine impulse force and (b) Comparison of the transient responses of vertical displacement w at node 2

Table 1 Six sets of four complex eigenvalues for lowest six undamped natural modes

Values	Undamped natural modes					
	1st	2nd	3rd	4th	5th	6th
Real	4.74	47.24	85.80	148.79	266.38	393.96
	4.74	47.24	85.80	148.79	266.38	393.96
	12.95	-4.20	-58.60	-136.47	-207.08	-392.61
	12.95	-4.20	-58.60	-136.47	-207.08	-392.61
Imaginary	-163.91	-1028.31	-2889.71	-5708.57	-9474.76	-15740.48
	163.91	1028.31	2889.71	5708.57	9474.76	15740.48
	-163.91	-1028.31	-2889.71	-5708.57	-9474.76	-15740.48
	163.91	1028.31	2889.71	5708.57	9474.76	15740.48

5. Damping properties

Next, we investigate the characteristics of damping and damped frequency. Figs. 7(a) and 7(b) represent the contour plots of non-dimensional real and imaginary parts of complex eigenvalue λ in Eq. (21) with respect to the viscous damping ratio ξ and the loss factor η . Referring to Fig. 7(a), the real value ($\sigma + a$) of complex eigenvalue which shows the damping of system increases in proportion to ξ and η . As ξ is a part of the damping value, it can be seen that ξ plays a big role, even for $\eta = 0$. By examining the contour lines, one can find out that those are in the relation of $0.5\eta + \xi = \xi_{total}$. This fact becomes more clear when ξ and η approach to 0, while ξ_{total}

such a relation, let us take Maclaurin series expansion of the real part a in Eq. (12) of complex eigenvalue. Then, we have

$$\begin{aligned}
 a(\xi, \eta) &= a(0, 0) + \left. \frac{\partial a}{\partial \xi} \right|_{0,0} \xi + \left. \frac{\partial a}{\partial \eta} \right|_{0,0} \eta \\
 &+ \frac{1}{2} \left(\left. \frac{\partial^2 a}{\partial \eta^2} \right|_{0,0} \eta + 2 \left. \frac{\partial^2 a}{\partial \xi \partial \eta} \right|_{0,0} \xi \eta + \left. \frac{\partial^2 a}{\partial \xi^2} \right|_{0,0} \xi^2 \right) + \dots
 \end{aligned}
 \tag{29}$$

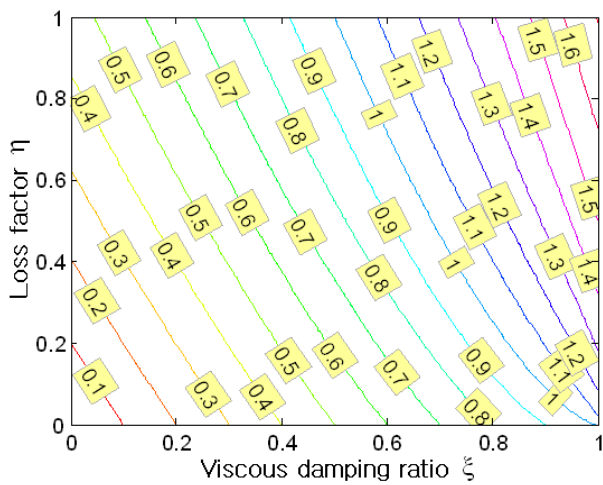
If ξ and η are sufficiently small, then we have

$$\lim_{\xi, \eta \rightarrow 0} a(\xi, \eta) \cong \omega_n 0.5\eta
 \tag{30}$$

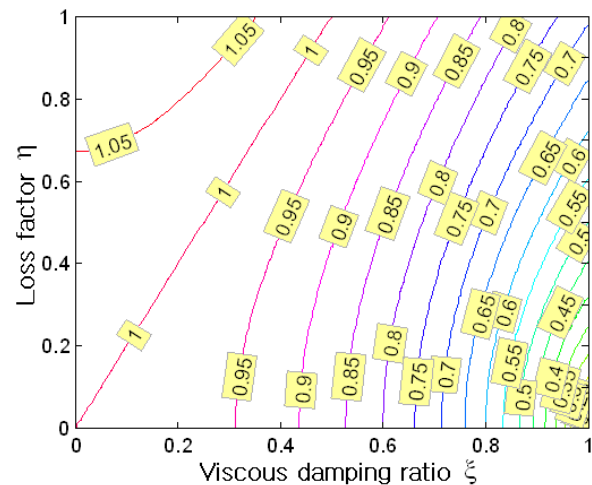
Reminding that $\sigma = \xi \omega_n$ from Eq. (21), it has been

justified that the non-dimensional damping $(\sigma + a) / \omega_n$

was also found that when the hysteretic damping η and



(a) non-dimensional damping $(\sigma + a) / \omega_n$



(b) non-dimensional damped natural frequency b / ω_n

Fig. 9 Contour plots with respect to ξ and η

satisfies the above relation $0.5\eta + \xi = \xi_{total}$ when ξ and η are sufficiently small. But, it can be seen from Fig. 9(a) that the contour lines deviate from the linear relation as ξ and η increase.

On the other hand, one can find a contour satisfying the relation of $\eta = 2\xi$ from Fig. 9(b), and there is no change in the damped frequency b along this contour. However, it can be seen that the damped frequency becomes higher or lower when the contours deviate from $\eta = 2\xi$. In general, the mass-spring-viscous damping system shows a decrease in damped frequency when damping is applied. However, when the complex stiffness (expressing hysteretic damping) is included, the damped frequency goes up or down depending on the values of complex stiffness and viscous damping. But, since the variance of damped frequency with respect to ξ and η ($0 < \eta, \xi < 0.5$) is small, when compared with the total damping ratio ξ , the effect of the damped frequency b on the response of system is negligible.

6. Conclusions

In this study, the unit impulse response of a vibration system with mixed hysteretic and viscous damping was obtained by Fourier integration, and the concept for determining the effective poles in a viscous-complex stiffness system was presented. And, using the effective poles, an equation for the unit impulse responses was derived by combining the vibration term and the residual term. It was observed that the non-causal phenomenon occurs because the sum of the initial value of vibration term and the residuals does not vanish. It was verified that this phenomenon occurs due to the discontinuity in the damping term of the hysteretic system in the frequency domain. It

the viscous damping ξ exist simultaneously, the damping properties are not expressed as a linear combination. Also, both the residual and the non-causal phenomenon, which are usually observed only in the hysteretic damping systems, vary depending on the value of viscous damping ξ , while the system's complex eigenvalues become different for different magnitudes of both damping coefficients ξ and η . But, when the individual damping coefficients are small, both the damping coefficients can be switched each other according to the relation of $\xi = 2\eta$, which was consistent with the earlier studies on the hysteretic damping (Crandall 1970, Henwood 2002).

This study also presented an approximation method to obtain the time response of system using Hilbert transform. The system governing equation in the time domain was separated into a real part and an imaginary part and transformed into the state space, to which the concept of effective pole was applied to obtain the time response. Using this approximation method, both the imaginary initial conditions and the forced vibration response can be obtained more simply than the conventional analytical method. However, for high damping systems in which the influence of the residual becomes larger and the non-causal phenomena increases, it is more desirable to use the analytical response equation presented in this paper because the state space method which restructures the vibration term becomes less accurate.

Acknowledgements

This work was supported by the Korea Institute of Machinery & Materials (No. NK205G, No. OS101H). This work was also supported by 2017 Hongik University Research Fund.

References

- Akbas, S.D. (2016), "Forced vibration analysis of viscoelastic nanobeams embedded in an elastic medium", *Smart Struct. Syst.*, **18**(6), 1125-1143.
- Amichi, K. and Atalla, N. (2009), "A new 3D finite element for sandwich beams with a viscoelastic core", *J. Vib. Acoust.*, **131**(2), 021010.
- Arfken, G.B. and Weber, H.J. (2005), *Mathematical Methods for Physicists*, Academic Press, London.
- Bae, S.H., Cho, J.R. and Jeong, W.B. (2016), "Free and transient responses of linear complex stiffness system by Hilbert transform and convolution integral," *Smart Struct. Syst.*, **17**(5), 753-771.
- Bae, S.H., Cho, J.R., Bae, S.R. and Jeong, W.B. (2014), "A discrete convolutional Hilbert transform with the consistent imaginary initial conditions for the time-domain analysis of five-layered viscoelastic sandwich beam", *Comput. Meth. Appl. Mech. Eng.*, **268**, 245-263.
- Barkanov, E., Rikards, R., Holste, C. and Täger, O. (2000), "Transient response of sandwich viscoelastic beams, plates, and shells under impulse loading", *Mech. Compos. Mater.*, **36**(3), 215-222.
- Bonisoli, E. and Mottershead, J.E. (2004), "Complex-damped dynamic systems in the time and frequency domains", *J. Shock Vib.*, **11**, 209-225.
- Chen, J.T. and You, D.W. (1999), "An integral-differential equation approach for the free vibration of a SDOF system with hysteretic damping", *Adv. Eng. Softw.*, **30**(1), 43-48.
- Crandall, S.H. (1970), "The role of damping in vibration theory", *J. Sound Vib.*, **11**(1), 3-18
- Feldman, M. (2011), *Hilbert Transform in Mechanical Vibration*, John Wiley & Sons, Ltd., Chichester, UK.
- Gaul, L., Bohlen, S. and Kempfle, S. (1985), "Transient and forced oscillations of systems with constant hysteretic damping", *Mech. Res. Commun.*, **12**(4), 187-201.
- Genta, G. and Amati, N. (2010), "Hysteretic damping in rotordynamics: An equivalent formulation", *J. Sound Vib.*, **329**(22), 4772-4784.
- Henwood, D.J. (2002), "Approximating the hysteretic damping matrix by a viscous matrix for modelling in the time domain", *J. Sound Vib.*, **254**(3), 575-593.
- Inaudi, J.A. and Makris, N. (1996), "Time-domain analysis of linear hysteretic damping", *Earthq. Eng. Struct. D.*, **25**(6), 529-545.
- Johansson, M. (1999), *The Hilbert Transform*, Master Thesis, Mathematics, Växjö University.
- Li, Z., Qiao, G., Sun, Z., Zhao, H. and Guo, R. (2012), "Short baseline positioning with an improved time reversal technique in a multi-path channel", *J. Mar. Sci. Appl.*, **11**(2), 251-257.
- Mohammadi, F. and Sedaghati, R. (2012), "Linear and nonlinear vibration analysis of sandwich cylindrical shell with constrained viscoelastic core layer", *Int. J. Mech. Sci.*, **54**(1), 156-171.
- Nashif, A.D., Jones, D.I.G. and Henderson, J.P. (1985), *Vibration Damping*, Wiley, New York.
- Padois, T., Prax, C., Valeau, V. and Marx, D. (2012), "Experimental localization of an acoustic sound source in a wind-tunnel flow by using a numerical time-reversal technique", *Acoust. Soc. Am.*, **132**(4), 2397.
- Soroka, W.W. (2012), "Note on the relations between viscous and structural damping coefficients," *J. Aeronaut. Sci.*, **16**(7), 409-410.
- Wang, Q., Yuan, S., Hong, M. and Su, Z. (2015), "On time reversal-based signal enhancement for active lamb wave-based damage identification", *Smart Struct. Syst.*, **15**(6), 1463-1479.
- Won, S.G., Bae, S.H., Cho, J.R., Bae, S.R. and Jeong, W.B. (2013), "Three-layered damped beam element for forced vibration analysis of symmetric sandwich structures with a viscoelastic core", *Finite Elem. Anal. Des.*, **68**, 39-51.
- Won, S.G., Bae, S.H., Jeong, W.B. and Cho, J.R. (2012), "Forced vibration analysis of damped beam structures with composite cross-section using Timoshenko beam element", *Struct. Eng. Mech.*, **43**(1), 15-30.
- Zhu, H., Hu, Y. and Pi, Y. (2014), "Transverse hysteretic damping characteristics of a serpentine belt: Modeling and experimental investigation", *J. Sound Vib.*, **333**(25), 7019-7035.

CC